Supporting Information

Modulating carbon quantum dots using multi-heteroatom doping as a bifunctional electrocatalyst for efficient oxygen and hydrogen evolution reactions in alkaline electrolytes

Nermeen S. Hafez,[a] El-Zeiny M. Ebeid [*a,b] Aya Khalifa [a] Saleh A. Azim [a] Abdelhamid El-Shaer[c] Mahmoud A. S. Sakr [b] and Mohamed Barakat Zakaria Hegazy [*a]

1. Experimental Section

1.1 Materials

(3-Aminopropyl) trimethoxysilane (APTMOS, 97%), urea (99%), citric acid monohydrate (99.5 %), phosphoric acid (H_3PO_4, 98%), sulfuric acid (H_2SO_4, 98%), Quinine Sulfate Dihydrate, potassium hydroxide (KOH, 99%), Isopropanol, and dimethylformamide (DMF, > 99%) were all purchased from Sigma-Aldrich (USA) and Fisher Scientific. Nafion perfluorinated resin solution (5 wt %) was purchased from Sigma-Aldrich, USA. Platinum, 20% on carbon, as a reference catalyst for HER and commercial Ni nanoparticals for OER were obtained from Alfa Aesar (Johnson Matthey, U.K.). Deionized water (18 MΩ cm) was used throughout the experiments. All reagents were of analytical grade, sourced from commercial suppliers, and used without further purification.

1.2 Instruments

Scanning electron microscopy (SEM) coupled with energy-dispersive X-ray spectroscopy (EDX) was used to confirm the elemental compositions of the prepared samples, using a JSM-6510LV at 20 kV. To evaluate the morphologies of the electrocatalysts, transmission electron microscopy (TEM) images were obtained with a JEOL 2100 microscope operating at 200 kV. The crystalline structure of the materials was identified through X-ray diffraction (XRD) analysis conducted at 35 kV and 25 mA using a Shimadzu diffractometer with Cu K_α radiation (λ = 1.54 Å). The scan rate was set to 2 min^{-1}, covering a 2θ range from 5° to 80°. The elemental composition was further analyzed using X-ray photoelectron spectroscopy (XPS) from Thermo Scientific, which utilized monochromatic Al K_α radiation (X-ray energy 1486.6 eV). The binding energies were calibrated to the C 1*s* signal at 284.8 eV. Raman spectroscopy was performed with a WITec alpha300 R setup, which included two laser sources: a 532 nm laser (maximum output of 30 mW) and a 785 nm laser (maximum output of 133 mW) to examine the structures of the produced materials. Fourier-transform infrared (FT-IR) spectroscopy was conducted in the range of 4000 to 400 cm^{-1} using a JASCO FT/IR-4100 spectrophotometer to analyze the functional groups in the prepared samples. The absorption spectrum was analyzed using a JASCO V-630 spectrophotometer, and a Brookhaven zeta potential/particle size analyzer was utilized to acquire additional results.

1.3 Electrochemical Setup

All electrochemical tests were conducted using a CHI660E workstation in a cell that was configured with three electrodes. The electrochemical cell setup consisted of a glassy carbon working electrode (3 mm diameter, CH Instruments) with a working area of 0.071 cm^2, an Ag/AgCl reference electrode (saturated KCl, CH Instruments), and a platinum wire serving as the counter electrode. The glassy carbon electrode was polished using Buehler alumina with particle sizes of 1.0 and 0.05 µm on Buehler polishing pads. In the representative experiments, for Si, N, P-CQDs, 5 ml of our diluted catalyst was well-dispersed in a 1.0 M KOH until a homogenous solution was obtained, while for N, P-CQDs, 3 ml from the dilute catalyst was transferred into 1.0 M KOH and stirred until a homogenous solution was obtained. The concentration of catalysts was fixed for all experiments.

To make the ink for the working electrode using Ni nanoparticles and Pt/C20% benchmark catalysts, 5 mg of the catalyst was well-dispersed using sonication for 15 min in a mixture of water and isopropanol (950 µL, 3:1 v/v) to establish a homogeneous solution. 50 µL of a 5 wt % Nafion™ perfluorinated resin solution as a binder was added to the previous suspension, and the mixture was sonicated continuously for an additional 10 min. After preparing the ink, 5 µL was applied to the GCE surface and allowed to dry at room temperature.

Linear sweep voltammetry (LSV) measurements were performed at a potential range between 1.0 V to 2.0 V vs. RHE for OER testing in 1.0 M KOH solution and 0.1 V to -1 V vs. RHE in 1.0 M KOH solution for HER with a scan rate of 50 mV s^{-1}. Tafel plots were derived from LSV curves around the onset potential region. The overpotential (η) was calculated according to the following formula: η (V) = E_{RHE} – 1.23 V for OER and η (V) = E_{RHE} – 0 V for HER. We calculated the exchange current density (J_0) from the intercept between the equilibrium potential at an overpotential of zero from the Tafel plot. Electrochemical impedance spectroscopy (EIS) measurements were performed at different potentials over a frequency range of 1 Hz to 100 kHz with an AC voltage amplitude of 5 mV to determine the charge transfer speed. Cyclic voltammetry (CV) measurements were performed between 1.0 to 1.4 V vs RHE at different scan rates (10 –100 mV.S^{-1}) for OER and between -0.4 to 1.1 V vs RHE at different scan rates (3 –100 mV.s^{-1}) for HER. Finally, a chronopotentiometry test was performed for 12 hours to determine the stability of the catalytic material in the case of OER at 100 $mAcm^{-2}$ and HER at -10 $mAcm^{-2}$.

Turnover frequency (*TOF*): A turnover frequency reflects the number of catalytic cycles that occur per active site in a unit of time. The formula, $TOF = ja / 4n^F$ was used to determine the turnover frequency (*TOF*) for OER, where *j* is the current density at a specific overpotential, *a* is the electrode's geometric surface area, 4 is the number of

electrons transferred in the OER, *n* is the number of moles of materials used for the OER, and *F* is Faraday's constant (96485 $Cmol^{-1}$) [1].

1.4 Computational methodology

The structural optimization of the studied systems was performed using density functional theory (DFT) as implemented in Gaussian 16 [2-6]. The hybrid B3LYP functional was selected for its proven reliability in similar materials, ensuring accurate electronic predictions [7]. The 6-31G basis set was employed to achieve a balance between computational efficiency and accuracy [8, 9], making it a widely adopted choice in related studies [10-13]. To account for van der Waals interactions between the studied compounds and adsorbed intermediates, Grimme's dispersion correction (gd3) was incorporated within the B3LYP functional [14].

1.5 Synthesis of Si, N, P tri-doped carbon quantum dots (Si, N, P-CQDs)

Si, N, P-CQDs were synthesized by a one-pot hydrothermal method. To get the highest fluorescence efficiency of the Si, N, P-CQDs, we changed APTMOS volume under the same reaction conditions. Single-factor-experiment results (**Fig. S1a and b**) indicated the obtained Si, N, P -CQDs have stronger fluorescence when the volume of APTMOS is 3.825 mL.

450 mg citric acid was mixed with 450 mg urea. To this mixture, 0.3 mL H_3PO_4, 3.83 ml (3-Aminopropyl) trimethoxysilane (APTMOS), and 30 mL dimethylformamide were added under an inert atmosphere. The solution was sonicated for 20 min, then transferred to a 50 mL Teflon-lined autoclave and heated for 12 h at 160 °C (Scheme 1). The solution changed from colorless to pale yellow during this process, indicating the formation of the Si, N, P-CQDs. The solution was centrifuged for 15 min at 12000 rpm with Legend Micro 21 centrifuge (Thermo Scientific, USA) to remove the non-fluorescent deposit. Then, the pH of the supernatant was adjusted to 7, and then the solution was subjected to dialysis against ultra-pure water through a dialysis membrane (1000 MWCO) for 24 h to remove small molecules. Afterward, the purified solution is diluted 10 times for further experiments.

1.6 Synthesis of N, P doped carbon quantum dots (N, P-CQDs)

N, P Carbon quantum dots were prepared following a modified literature procedure [15]. In a typical procedure, 450 mg citric acid and 450 mg urea were mixed together, and then 0.3 mL H_3PO_4 and 30 mL dimethylformamide were added under an inert atmosphere. The solution was sonicated for 20 min and then transferred to a 50 mL Teflon-lined autoclave for one-pot hydrothermal treatment at 160 °C for 12 h (Scheme 1). During this process, the solution changed from colorless to red, indicating the formation of the N, P-CQDs. The solution was centrifuged for 15 min at 12000 rpm with Legend

Micro 21 centrifuge (Thermo Scientific, USA) to remove the non-fluorescent precipitates. Then, the supernatant was adjusted to pH 7, followed by dialysis against ultra-pure water through a dialysis membrane (1000 MWCO) for 24 h to remove small molecules. Afterwards, the solution was diluted 10 times for further experiments.

1.7 Fluorescence quantum yield determination of Si, N, P CQDs

The standard was quinine sulfate in 0.1 M H_2SO_4 (Φ = 0.54). The QY of Si, N, P CQDs was evaluated at 380 nm excitation wavelength for Si, N, P CQDs using a comparative method following the equation [16]:

$$\Phi_s = \Phi_{std} \times \left(\frac{I_s}{I_{std}}\right) \times \left(\frac{A_{std}}{A_s}\right) \times \left(\frac{\eta_s}{\eta_{std}}\right)^2$$

Where Φ_s is the quantum yield of Si, N, P CQDs, Φ_{std} is the quantum yield of quinine sulfate, I_s is the area under the PL curve of Si, N, P CQDs, I_{std} is the area under the PL curve of quinine sulfate, A_s is the absorbance of Si, N, P CQDs, while A_{std} is the absorbance of quinine sulfate at the excitation wavelength. η_s and η_{std} are the refractive indices of Si, N, P CQDs and quinine sulfate, respectively. The value of η_s / η_{std} is 1 for those two solutions. During the analysis, the absorbance was reduced to less than 0.1 to avoid reabsorption by both CQD and quinine sulfate.

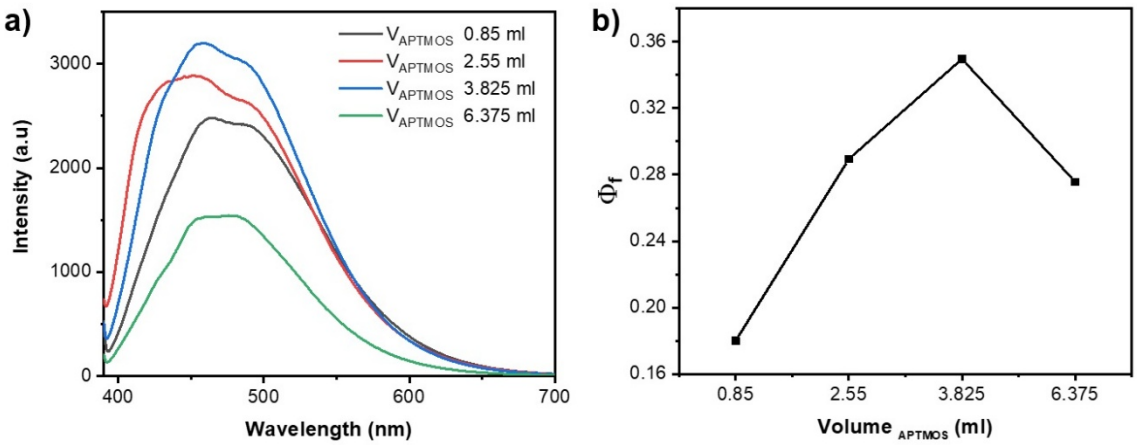

Fig. S1 a) The emission spectra of Si,N,P-CQDs synthesized at different volumes of APTMOS and b) Fluorescence quantum yield of Si, N, P -CQDs as a function of APTMOS volume.

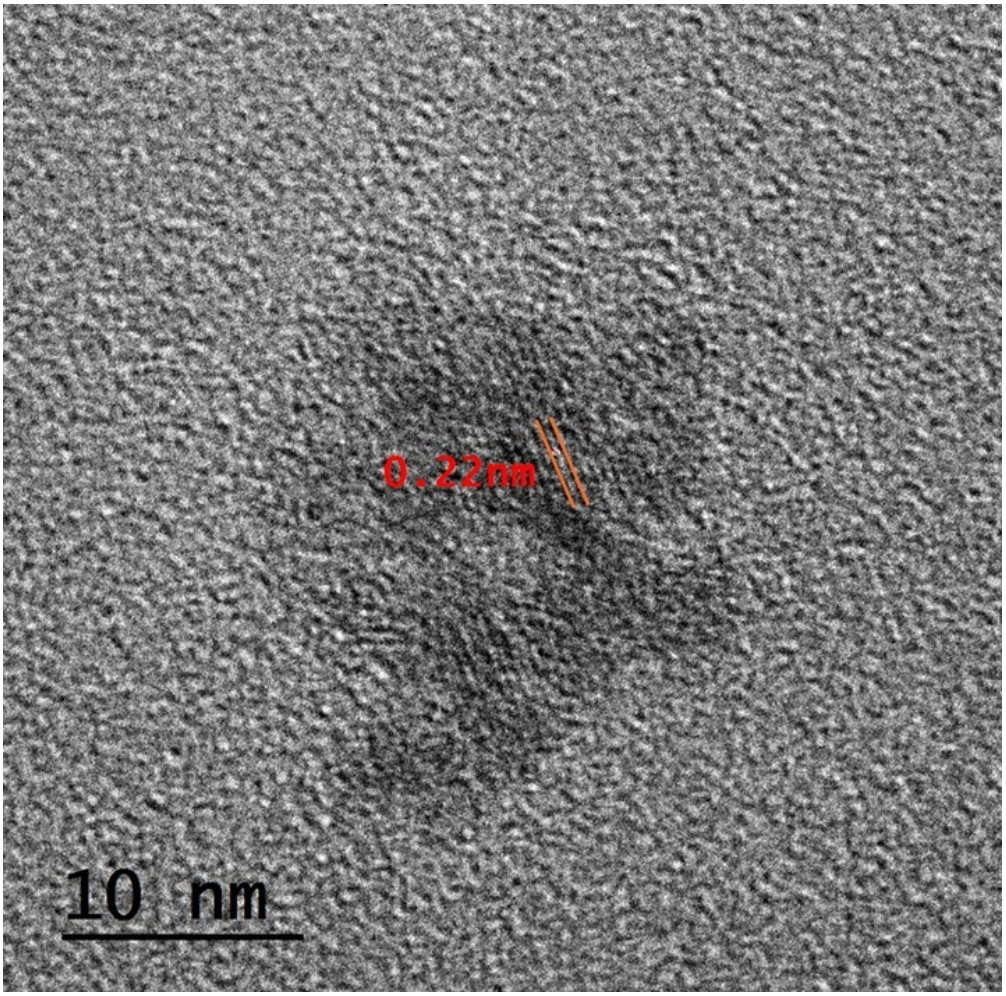

Fig. S2 HRTEM image of one particle in the Si, N, P-CQD sample.

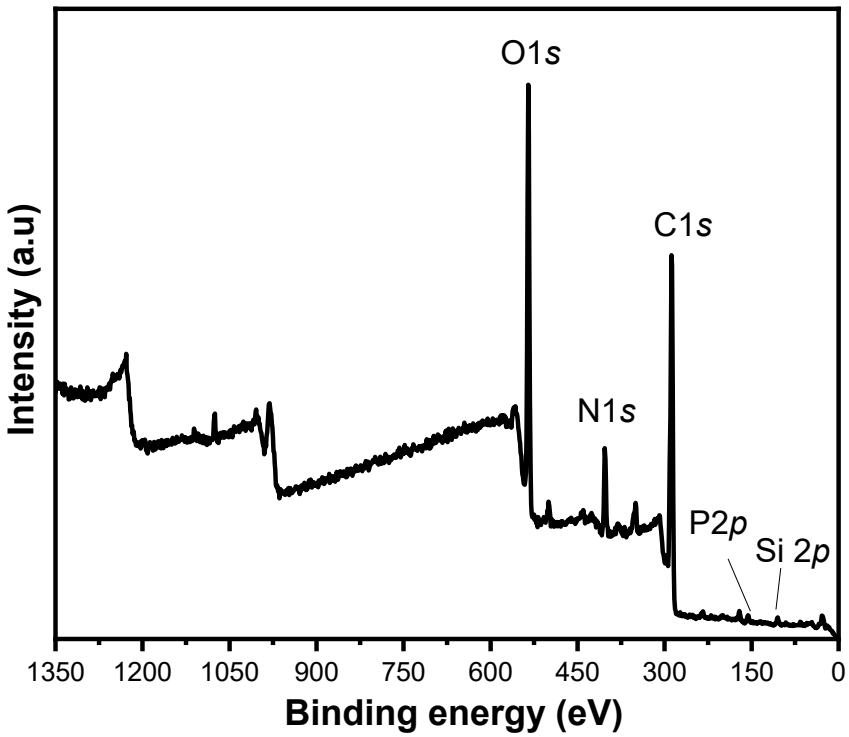

Fig. S3 wide scan XPS spectrum of Si,N,P-CDQs sample.

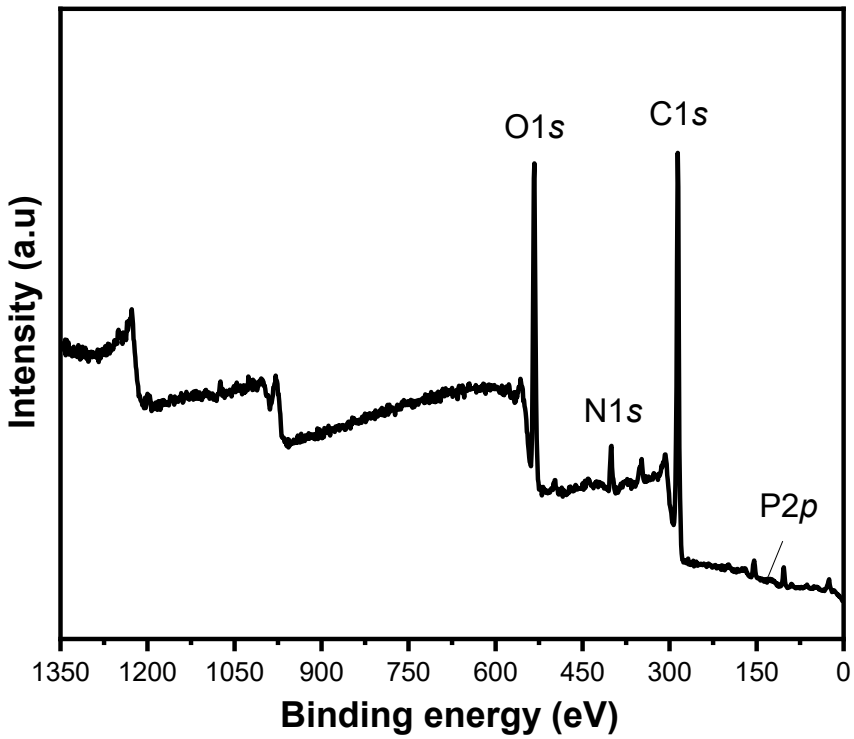

Fig. S4 wide scan XPS spectrum of N,P-CDQs sample.

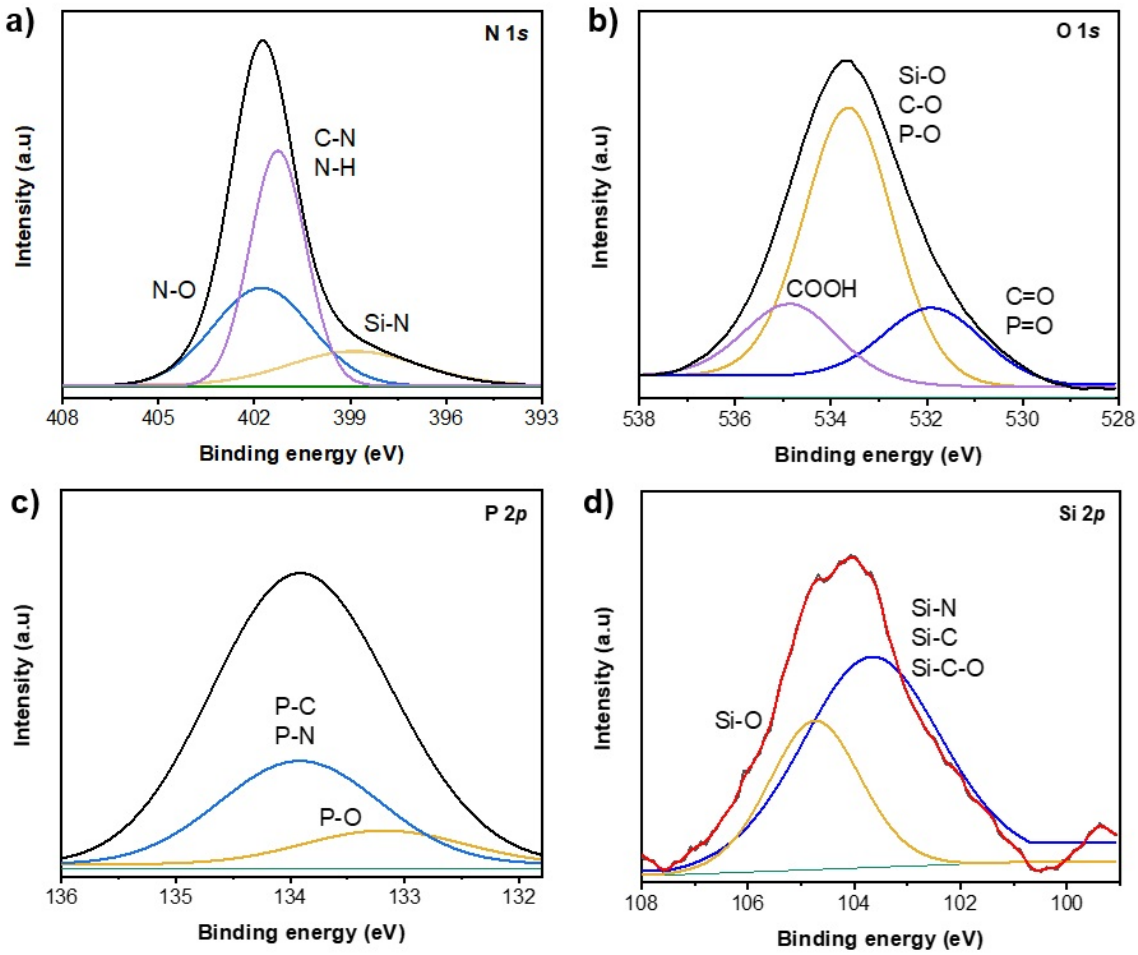

Fig. S5 High-resolution XPS spectra a) N 1*s*, b) O 1*s*, c) P 2*p*, and d) Si 2*p* orbitals in of Si,N,P-CQDs.

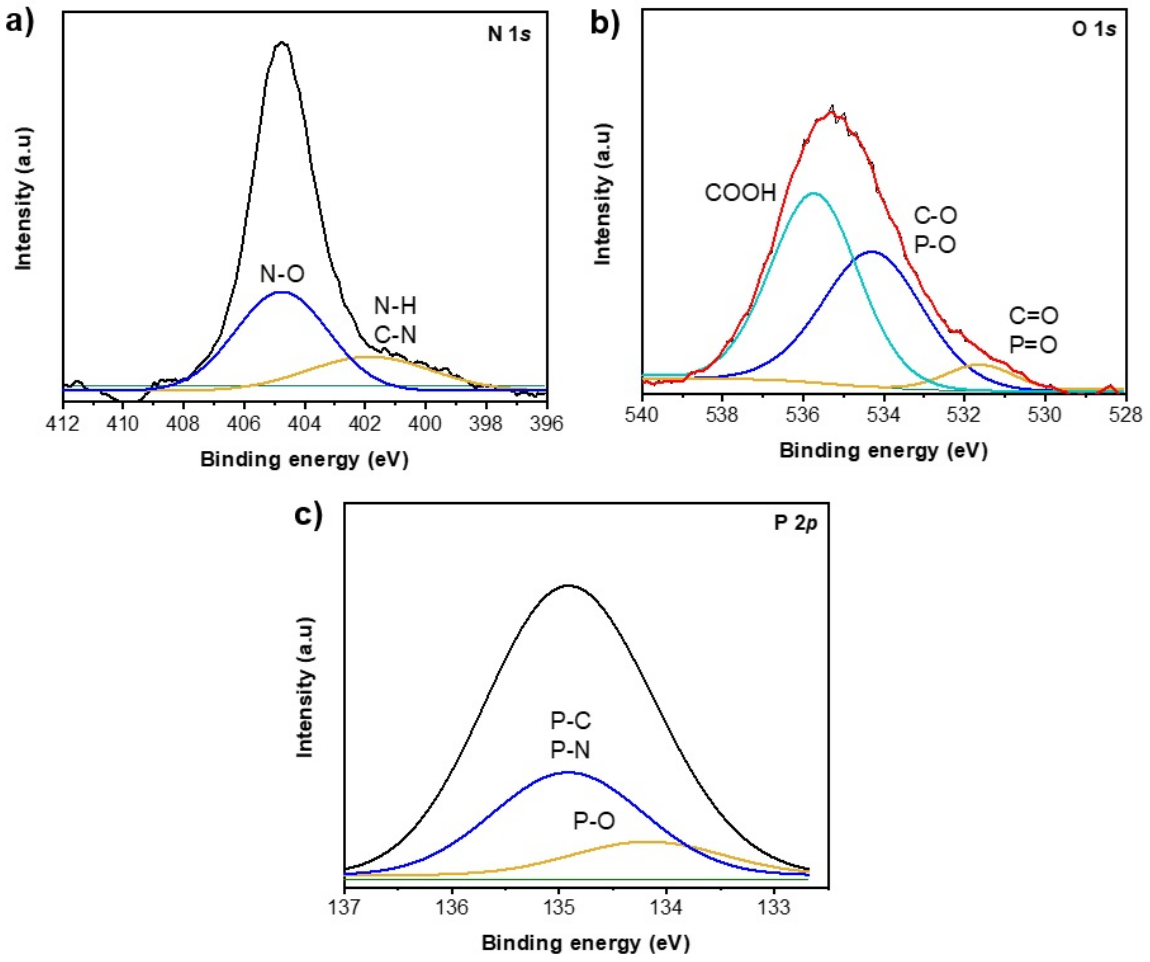

Fig. S6 High-resolution XPS spectra a) N 1*s*, b) O 1*s*, and c) P 2*p* in of N,P-CQDs.

.

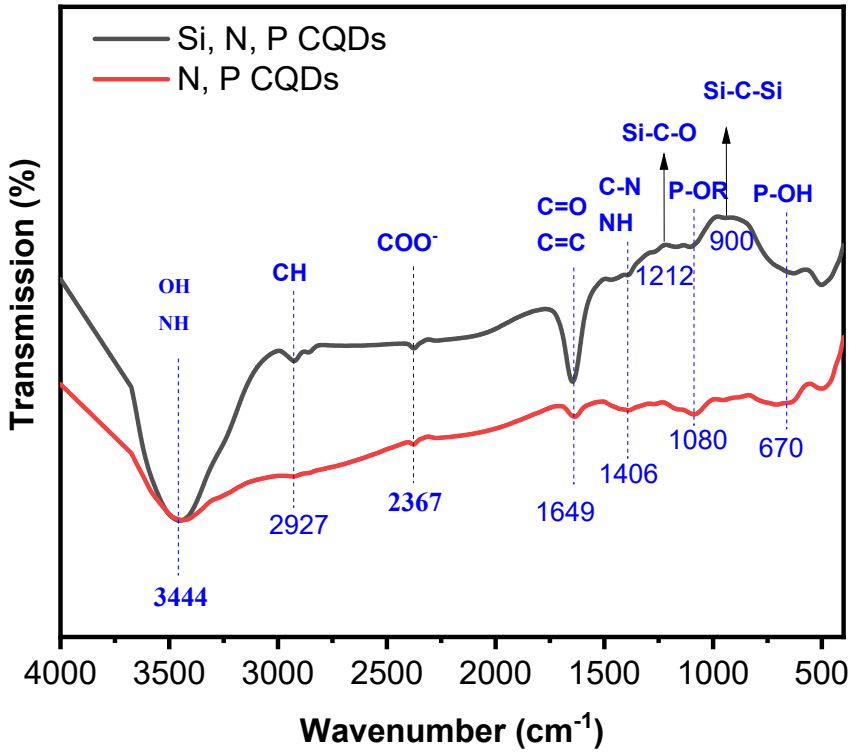

Fig. S7 IR spectrum of Si, N, P-CQDs and N, P-CQDs.

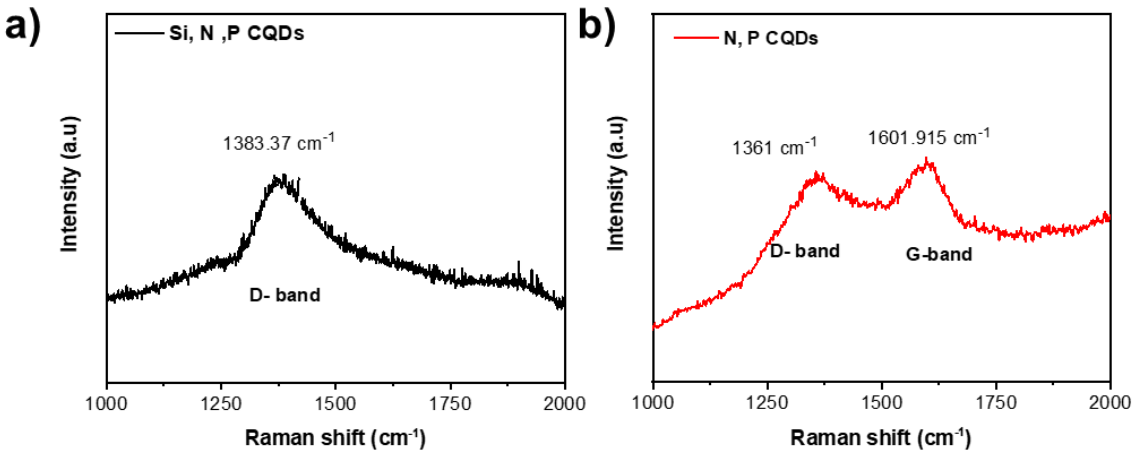

Fig. S8 Raman spectra of a) Si, N, P-CQDs and b) N, P-CQDs.

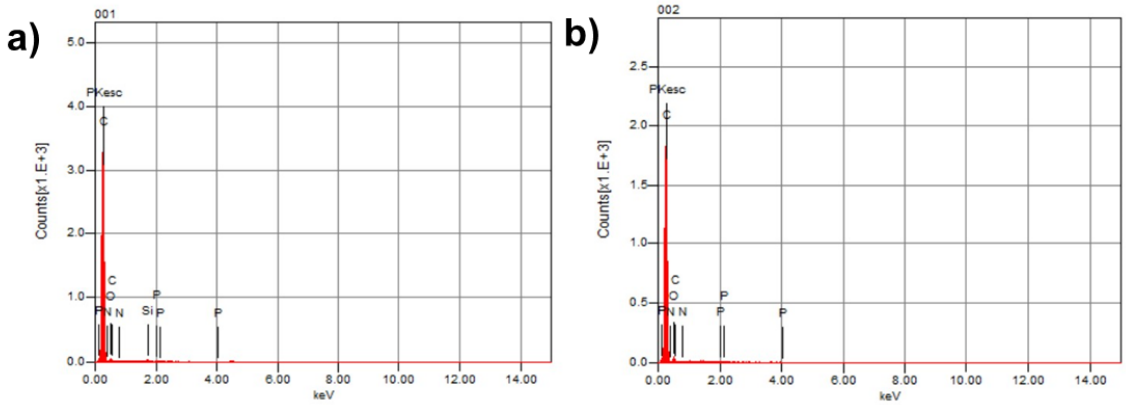

Fig. S9 EDX spectra of a) Si, N, P-CQDs and b) N, P-CQDs.

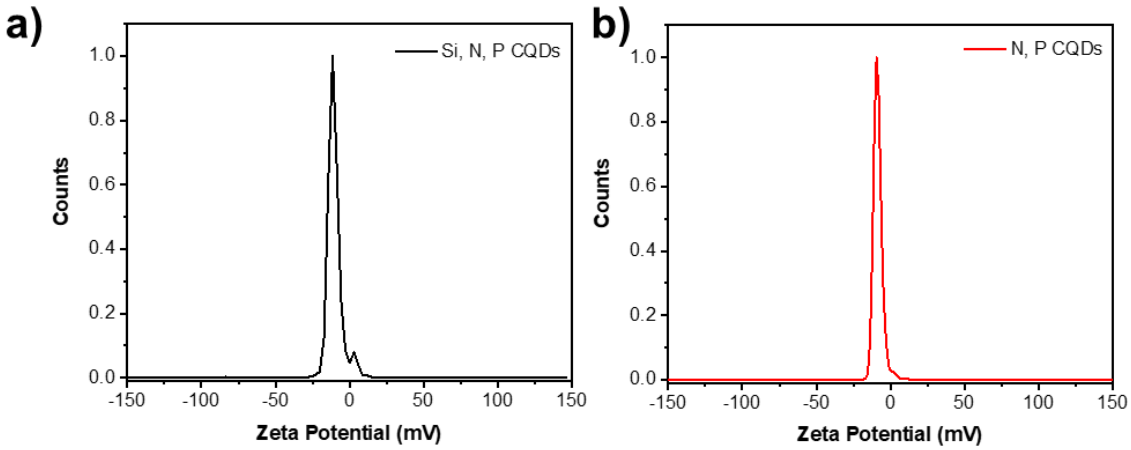

Fig. S10 Zeta potential of a) Si, N, P-CQDs and b) N, P-CQDs.

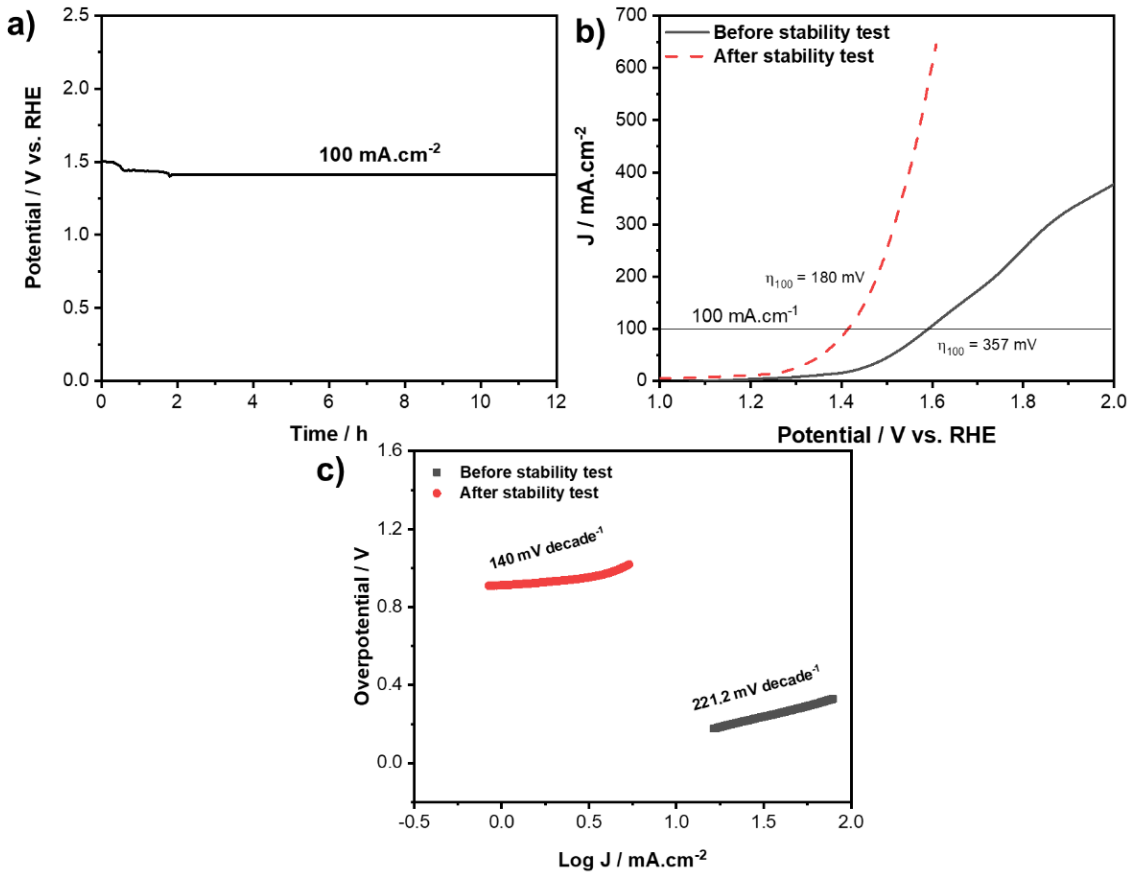

Fig. S11 a)Chronopotentiometry test of Si, N, P-CQDs at 100 mA. cm^{-2} for 12 h for OER. b) Polarization curves of Si, N, P-CQDs at a scan rate of 50 mVs^{-1} in 1.0 M KOH aqueous solution, and c) the corresponding Tafel plots of Si, N, P-CQDs before and after chronopotentiometry test for OER.

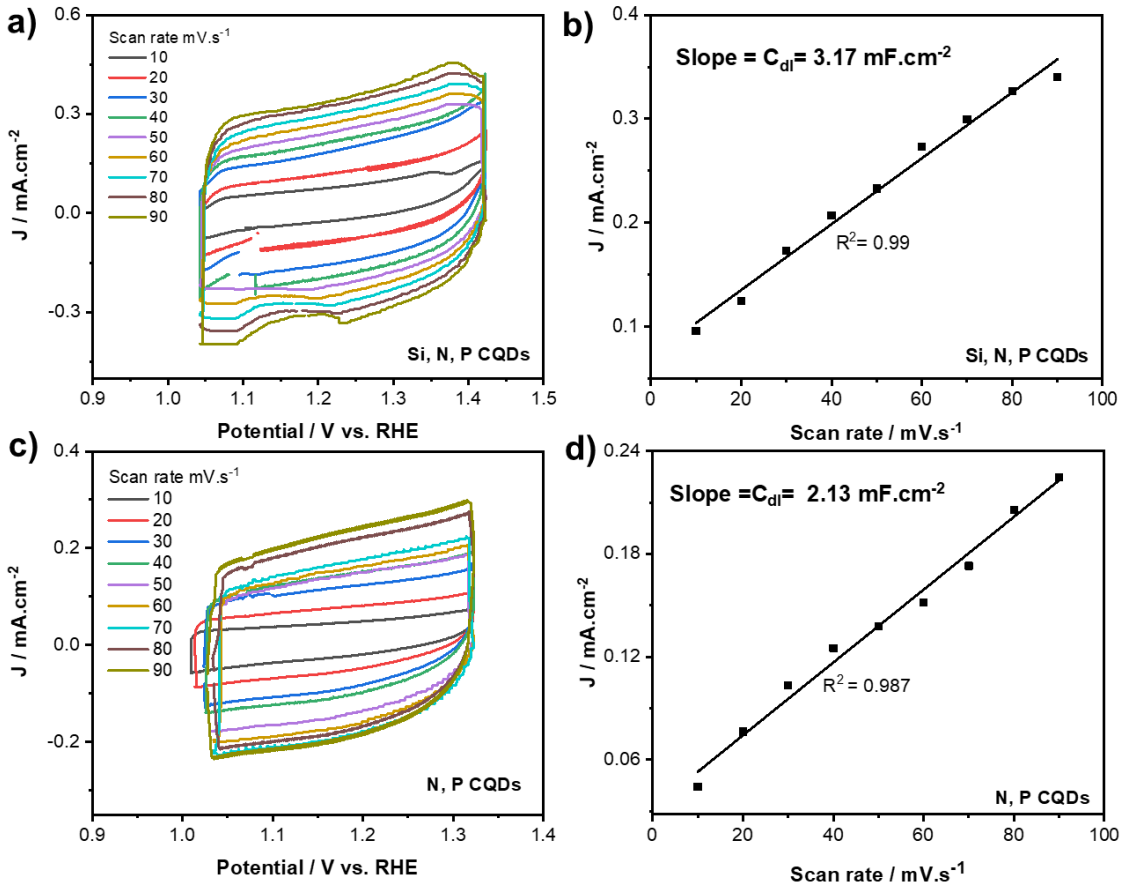

Fig. S12 CV curves a, c) at 10, 20,30, 40, 50, 60, 70, 80, and 90 mV s^{-1} in 1.0 M KOH solution and b, d) current density vs. scan rate plots of Si, N, P-CQDs and N, P-CQDs using glassy carbon electrode as a working electrode.

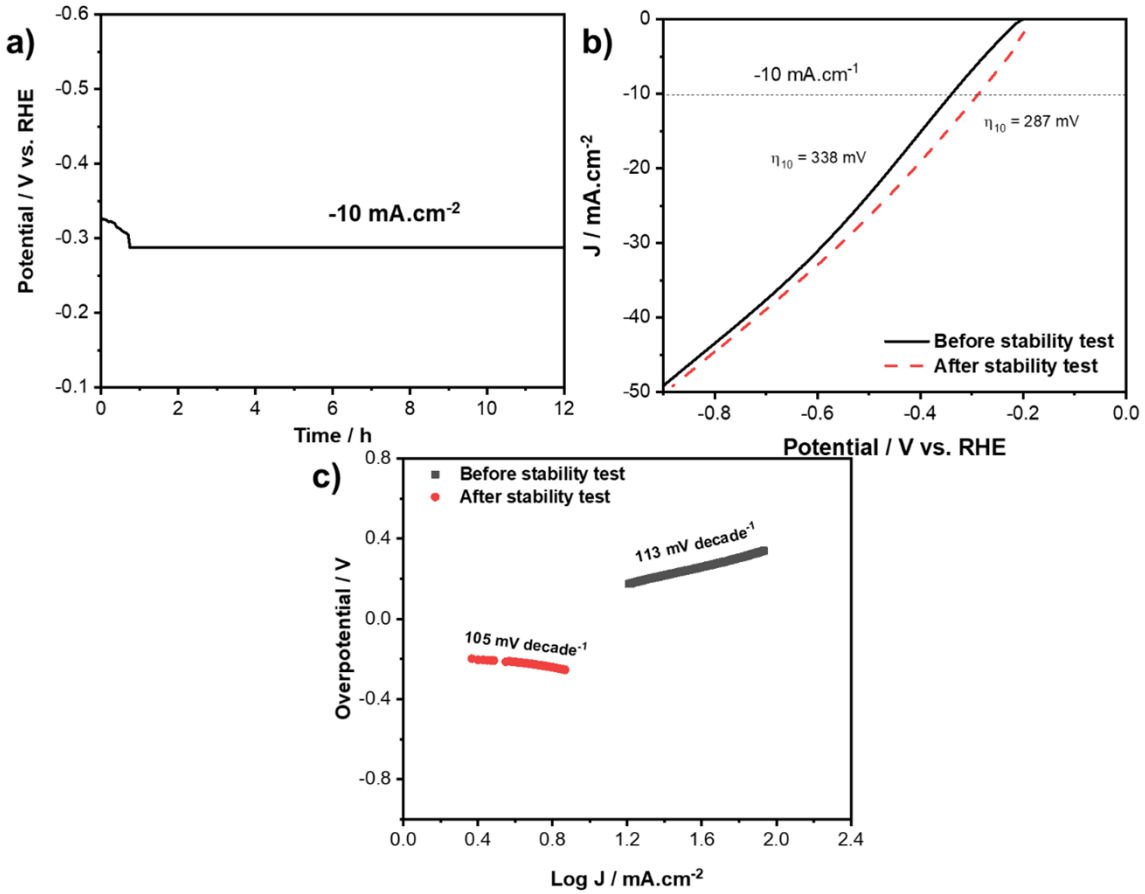

Fig. S13 a) Chronopotentiometry test of Si, N, P-CQDs at -10 mA. cm^{-2} for 12h for HER. b) Polarization curves of Si, N, P-CQDs at a scan rate of 50 mVs^{-1} in 1.0 M KOH aqueous solution, and c) the corresponding Tafel plots of Si, N, P-CQDs before and after chronopotentiometry test for HER.

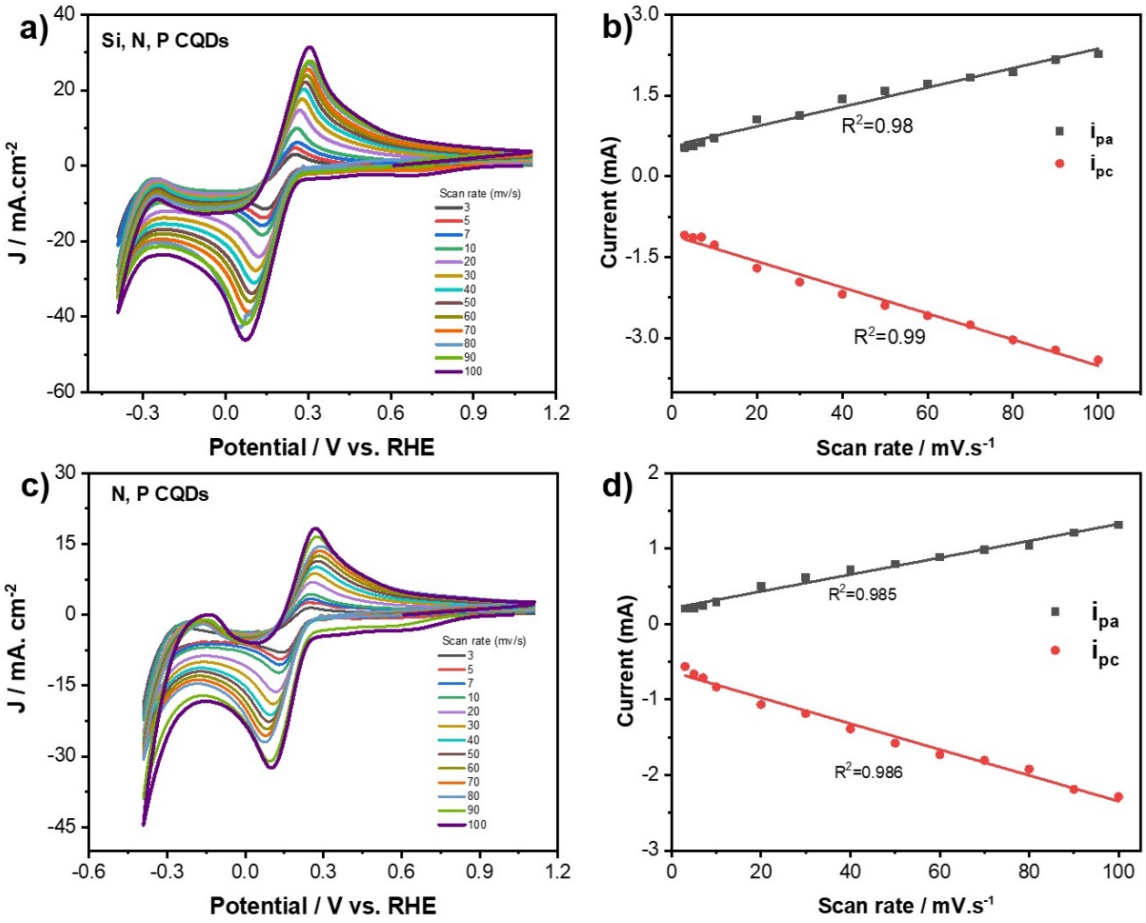

Fig. S14 CV curves a,c) at 3, 5, 7, 10, 20, 30, 40, 50, 60, 70, 80, 90, and 100 mVs^{-1} in 1.0 M KOH solution and b, d) current vs. scan rate plots of Si, N, P-CQDs and N, P-CQDs using a glassy carbon electrode as a working electrode.

Table S1 A comparison of the electrocatalytic activity of Si, N, P-CQDs and N, P-CQDs towards OER with other electrocatalysts was recently published

Catalysts	**Overpotential (η_{10}, mV)**	**Tafel slope ($mV.dec^{-1}$)**	**Electrolytes**	**Catalysis type**	**Reference**
Co-Et	672	114	0.1M KOH	Heterogenous	[17]
Co-Pr	724	151	0.1M KOH	Heterogenous	[17]
FCl-CQDs/VG	393	335	1M KOH	Heterogenous	[18]
FCNSSi	316	70	1M KOH	Heterogenous	[19]
FCNSP	419	76	1M KOH	Heterogenous	[20]
FCNSN	390	64	1M KOH	Heterogenous	[20]
FCNSNP	349	51	1M KOH	Heterogenous	[20]
Ni/NiS/P, N, S-rGO	155	135	1M KOH	Heterogenous	[21]
(2,2'-bipyridine)CuII$(OH)_2$	750	-	0.1M NaOH/NaOAc	Homogenous	[22]
6,6´hydroxyl 2,2´bipyridine)CuII$(OH)_2$	530	-	0.1M NaOH/NaOAc	Homogenous	[23]
([Ni(meso-Me_6L)]$(ClO_4)_2$ L=5,5,7,12,12,14 hexamethyl-1,4,8,11-tetraazacyclotetradecane	170	-	0.1M phosphate buffer (pH=7)	Homogenous	[24]
$(Me_4N)_2$(NiL) L=o-phenylenebis(N'-methyloxamidate)	480	-	0.1M phosphate buffer (pH=11)	Homogenous	[25]

Table S2 A comparison of the electrocatalytic activity of Si, N, P-CQDs and N, P-CQDs towards HER with other electrocatalysts was recently published

Catalysts	**Overpotential η_{10}, mV**	**Tafel slope mVdec^{-1}**	**Electrolytes**	**Catalysis type**	**Reference**
Co-Et	1050	-	TFA TFA=Trifluoroacetic acid	Homogenous	[17]
Co-Pr	920	-	TFA	Homogenous	[17]
FCl-CQDs/VG	171	87	1M KOH	Heterogenous	[18]
(Ar_4)PNi(II)	∼880	-	TFA+ CH_3CN	Homogenous	[26]
[Ni(CAM)(dppe)] CAM=cyanoacetamidedithiolate dppe=1,2- bis-(diphenylphosphinoethane)	1029	-	TFA/CH_3CN	Homogenous	[27]
[Ni(CAM)(dppf)] CAM=cyanoacetamidedithiolate dppf=1,10-bis-(diphenylphosphino)ferrocene)	802	-	TFA/CH_3CN	Homogenous	[27]
[Ni(CAM)$(PPh_3)_2$] CAM=cyanoacetamidedithiolate PPh_3=triphenylphosphane	1155	-	TFA/CH_3CN	Homogenous	[27]
Ni[$P_2S_2C_2(C_6H_4R\text{-}P)_2$] R= CH_3	1000	-	TAF/DMF	Homogenous	[28]
Ni[$P_2S_2C_2(C_6H_4R\text{-}P)_2$] R= F	950	-	TAF/DMF	Homogenous	[28]
Ni[$P_2S_2C_2(C_6H_4R\text{-}P)_2$] R= H	970	-	TAF/DMF	Homogenous	[28]
Ni[$P_2S_2C_2(C_6H_4R\text{-}P)_2$] R= Br	910	-	TAF/DMF	Homogenous	[28]
Ni(bpy)(mp) mp=2-hydroxythiophenol bpy = 2,2´-bipyridine	580	-	TAF/DMF	Homogenous	[29]
Ni(dmbpy)(mp) mp=2-hydroxythiophenol dmbpy = 4,4´ -dimethyl-2,2´ -bipyridine	720	-	TAF/DMF	Homogenous	[29]
Ni nanoparticle	180	111	1 M NaOH	Heterogenous	[30]
Co_9S_8@NOSC NOSC: N-, O-, and S-tridoped carbon	320	105	1 M KOH	Heterogenous	[31]
p-WP_2	175	131	1 M KOH	Heterogenous	[32]

Table S3 Comparison of the redox properties of Si, N, P-CQDs and N, P-CQDs in 1.0 M in KOH at a scan rate of 100 mV s^{-1}

Catalyst	i_{pa}(mA)	i_{pc} (mA)	i_{pa}/i_{pc}	E_{pa} (V)	E_{pc} (V)	*TOF* (s^{-1})
Si, N, P-CQDs	2.25	-3.39	-0.663	0.3	0.07	0.0852
N, P-CQDs	1.33	-2.29	-0.58	0.267	0.1	0.0652

E_{pc} and i_{pc} are the reduction potential and the reduction current

E_{pa} and i_{pa} are the oxidation potential and the oxidation current

TOF is a turnover frequency

References

1. M. L. Helm, M. P. Stewart, R. M. Bullock, M. R. DuBois and D. L. DuBois, *Science*, 2011, **333**, 863-866.
2. H. Abdelsalam, V. A. Saroka, M. M. Atta, O. H. Abd-Elkader, N. S. Zaghloul and Q. Zhang, *Crystals* 2022, **12**, 1684.
3. H. Abdelsalam, T. Espinosa-Ortega and I. Luk'yanchuk, *Low Temperature Physics*, 2015, **41**, 396-400.
4. O. H. Abd-Elkader, H. Abdelsalam, M. A. S. Sakr, A. A. Shaltout and Q. Zhang, *Crystals*, 2023, **13**, 994.
5. M. A. S. Sakr and M. A. Saad, *Journal of Molecular Structure*, 2022, **1258**, 132699.
6. M. Frisch, G. Trucks, H. Schlegel, G. Scuseria, M. Robb, J. Cheeseman, G. Scalmani, V. Barone, G. Petersson and H. Nakatsuji, *Inc., Wallingford CT*, 2016, **3**.
7. K. Raghavachari, *Theoretical Chemistry Accounts*, 2000, **103**, 361-363.
8. Y. Y. Rusakov, Y. A. Nikurashina and I. Rusakova, *The Journal of Chemical Physics*, 2024, **160**.
9. S. F. Machado, G. G. Camiletti, A. C. Neto, F. E. Jorge and R. S. Jorge, *Molecular Physics*, 2009, **107**, 1713-1727.
10. N. H. Teleb, M. A. Sakr, M. A. Saad, O. H. Abd-Elkader, H. Abdelsalam and Q. Zhang, *Chinese Journal of Physics*, 2025, **94**, 274-286.
11. M. A. Saad, M. A. S. Sakr, N. H. Teleb, O. H. Abd-Elkader, H. Abdelsalam and Q. Zhang, *Chemical Physics Impact*, 2024, **8**, 100620.
12. H. Abdelsalam, W. O. Younis, V. A. Saroka, N. H. Teleb, S. Yunoki and Q. Zhang, *Physical Chemistry Chemical Physics*, 2020, **22**, 2566-2579.
13. H. Abdelsalam, M. A. S. Sakr, V. A. Saroka, O. H. Abd-Elkader and Q. Zhang, *Surfaces and Interfaces*, 2023, **40**, 103109.
14. S. Grimme, J. Antony, S. Ehrlich and H. Krieg, *The Journal of chemical physics*, 2010, **132**, 154104.
15. K. M. Omer, D. I. Tofiq and A. Q. Hassan, *Microchimica Acta*, 2018, **185**, 1-8.
16. M. P. Sk and A. Chattopadhyay, *RSC Advances*, 2014, **4**, 31994-31999.
17. D. Srivastava, O. Daniel, A. Kushwaha, G. Kociok-Köhn, S. W. Gosavi, R. Chauhan, M. Muddassir and A. Kumar, *New Journal of Chemistry*, 2024, **48**, 12217-12226.
18. Y. An, Z. Ren, Y. Kong, Y. Tian, B. Jiang and F. Shaik, *International Journal of Hydrogen Energy*, 2024, **58**, 633-645.
19. M. B. Z. Hegazy, L. Bahri, D. Tetzlaff, S. A. Sanden and U.-P. Apfel, *Energy Advances*, 2023, **2**, 1190-1203.
20. M. B. Z. Hegazy, K. Harrath, D. Tetzlaff, M. Smialkowski, D. Siegmund, J. Li, R. Cao and U.-P. Apfel, *iScience*, 2022, **25**, 105148.
21. M. B. Z. Hegazy, M. R. Berber, Y. Yamauchi, A. Pakdel, R. Cao and U.-P. Apfel, *American Chemical Society Applied Materials Interfaces*, 2021, **13**, 34043-34052.
22. S. M. Barnett, K. I. Goldberg and J. M. Mayer, *Nature chemistry*, 2012, **4**, 498-502.
23. T. Zhang, C. Wang, S. Liu, J.-L. Wang and W. Lin, *Journal of the American Chemical Society*, 2014, **136**, 273-281.
24. M. Zhang, M. T. Zhang, C. Hou, Z. F. Ke and T. B. Lu, *Angewandte Chemie*, 2014, **126**, 13258-13264.
25. D. K. Dogutan, R. McGuire Jr and D. G. Nocera, *Journal of the American Chemical Society*, 2011, **133**, 9178-9180.

26. S. Xue, X. Lv, N. Liu, Q. Zhang, H. Lei, R. Cao and F. Qiu, *Inorganic Chemistry*, 2023, **62**, 1679-1685.
27. S. Srivastava, D. Omoding, A. Kushwaha, G. Kociok-Köhn, S. Ahmed and A. Kumar, *New Journal of Chemistry*, 2024, **48**, 20268-20279.
28. L. Chen, T. Li, B. Xie, C. Lai, R.-W. Ji, J.-Y. He, J.-X. Cao, M.-N. Liu, W. Li and D.-L. Zhang, *Catalysis Science & Technology*, 2023, **13**, 3655-3666.
29. F. Kamatsos, K. Bethanis and C. A. Mitsopoulou, *Catalysts*, 2021, **11**, 401.
30. S. A. Abbas, M. I. Iqbal, S.-H. Kim and K.-D. Jung, *Electrochimica Acta*, 2017, **227**, 382-390.
31. S. Huang, Y. Meng, S. He, A. Goswami, Q. Wu, J. Li, S. Tong, T. Asefa and M. Wu, *Advanced functional materials*, 2017, **27**, 1606585.
32. M. Pi, T. Wu, W. Guo, X. Wang, D. Zhang, S. Wang and S. Chen, *Journal of Power Sources*, 2017, **349**, 138-143.